Biology Direct

RESEARCH

Open Access

METTL3 in cancer-associated fibroblasts-derived exosomes promotes the proliferation and metastasis and suppresses ferroptosis in colorectal cancer by eliciting ACSL3 m6A modification

Hongtao Ren[1], Mincong Wang[1], Xiulong Ma[1], Lei An[1], Yuyan Guo[1] and Hongbing Ma[1*]

Abstract

Background Cancer-associated fibroblasts (CAFs) have been reported that can affect cancer cell proliferation, metastasis, ferroptosis, and immune escape. METTL3-mediated N6-methyladenine (m6A) modification is involved in the tumorigenesis of colorectal cancer (CRC). Herein, we investigated whether METTL3-dependent m6A in CAFs-derived exosomes (exo) affected CRC progression.

Methods qRT-PCR and western blotting analyses detected levels of mRNAs and proteins. Cell proliferation and metastasis were evaluated using MTT, colony formation, transwell, and wound healing assays, respectively. Cell ferroptosis was assessed by detecting cell viability and the levels of Fe+, reactive oxygen species, and glutathione after erastin treatment. Exosomes were isolated from CAFs by ultracentrifugation. The m6A modification profile was determined by methylated RNA immunoprecipitation assay and the interaction between METTL3 and ACSL3 (acyl-CoA synthetase 3) was verified using dual-luciferase reporter assay. Animal models were established for in vivo analysis.

Results CAFs promoted CRC cell proliferation and metastasis, and suppressed cell ferroptosis. METTL3 was enriched in CAFs and was packaged into exosomes. The m6A modification and METTL3 expression were increased in CRC samples. Knockdown of METTL3 in CAFs-exo suppressed CRC cell proliferation and metastasis, and induced cell ferroptosis. Mechanistically, METTL3 induced ACSL3 m6A modification and stabilized its expression. The anticancer effects mediated by METTL3-silenced CAFs-exo could be rescued by ACSL3 overexpression. Moreover, in vivo assay also showed that CAFs-exo with decreased METTL3 could hinder CRC growth and metastasis in mice models.

Conclusion CAFs promoted the proliferation and metastasis, and restrained the ferroptosis in CRC by exosomal METTL3-elicited ACSL3 m6A modification.

Keywords Ferroptosis, CRC, Exosomes, m6A, CAFs, METTL3, ACSL3

*Correspondence:
Hongbing Ma
mhbxian2024@126.com
[1]Department of Radiotherapy, Second Affiliated Hospital of Xi'an Jiaotong University, No. 57, Siwu Road, Xi'an City, Shaanxi 710004, China

Introduction

Colorectal cancer (CRC) is the second leading cause of cancer-related deaths throughout the world [1]. Due to the unobvious, non-typical or specific clinical signs at the early stage, the early diagnosis rate of CRC is low, and the 5-year survival rate of advanced CRC patients, losing the opportunity for radical treatment, is only around 10% [2, 3]. Accordingly, probing the pathogenesis of CRC and developing effective therapies to improve the prognosis of CRC patients are indispensable.

To date, increasing proofs hint at the significant role of the tumor microenvironment (TME) in cancer progression [4]. Cancer-associated fibroblasts (CAFs) are essential components of TEM with important plasticity and heterogeneity, activated CAFs can influence cancer cell proliferation, metastasis, immune escape, angiogenesis, therapeutic resistance and drug access by extracellular matrix (ECM) remodeling and production of soluble factors, such as growth factors, cytokines, chemokines or other effector molecules [5–8]. In addition, exosomes seem to play a significant role in the crosstalk between tumor cells and TME [9]. CAFs-originated exosomes have been confirmed to regulate cancer occurrence, development, and metastasis by transferring numerous signaling factors [10–12]. For example, CAFs conferred gemcitabine resistance and restrained ferroptosis in pancreatic cancer cells by suppressing ACSL4 expression via secreting miR-3173-5p through exosomes [13]. CAF-originated exosomes enhanced breast cancer metastasis and proliferation by secreting miR-500a-5p to bind to USP28 [14]. Exosomal miR-345-5p derived from CAFs facilitated cell oncogenic phenotypes and CRC growth [15]. Therefore, targeting CAF-derived exosomes or interfering with their activities may be a promising therapeutic strategy for CRC.

Methyltransferase-like 3 (METTL3), one of the RNA methyltransferases, is the sole catalytic subunit of the methyltransferase complex, which catalyzes the N6-methyladenosine (m6A) methylation of mRNA, thereby affecting the stability and translation of mRNA [16, 17]. Currently, METTL3-induced m6A modification has been verified to play a significant role in tumorigenesis. For instance, METTL3 degraded DCP2 by inducing DCP2 m6A methylation, and then conferred chemoresistance by inducing mitochondrial autophagy in small cell lung cancer [18]. METTL3 induced PD-L1 m6A modification in an IGF2BP3-dependent manner, thereby promoting immune escape in breast cancer [18]. In CRC, METTL3 enhanced the migratory and proliferative abilities of cancer cells by stabilizing SNHG1 in the m6A-dependent manner [19]. In addition, Pan et al. showed that METTL3-mediated m6A methylation boosted miR-181b-5p process in CAFs-derived exosomes, which then enhanced 5-FU resistance in CRC [20]. However, whether METTL3-dependent m6A in CAFs-derived exosomes affects CRC oncogenic phenotypes remains unclear.

Herein, this study focused on exploring the action of CAFs-derived exosomes in CRC cells, and found that CAF-derived exosomes promoted the proliferation and metastasis and inhibited ferroptosis in CRC cells in vitro and also impeded CRC growth and metastasis in vivo, which might be related to exosomal METTL3-elicited m6A modification.

Materials and methods

Clinical samples

In total, 29 pairs of CRC samples and para-carcinoma tissues were obtained by surgery from CRC patients in the Second Affiliated Hospital of Xi'an Jiaotong University. The samples were preserved at -80℃. Every patient was informed prior to the study. This study was approved by the institutional ethics committee of the Second Affiliated Hospital of Xi'an Jiaotong University based on the Declaration of Helsinki.

Cell culture

Human CRC cell lines LoVo and HCT-116 and normal NCM460 cell line were purchased from FuHeng Biotechnology (Shanghai, China), and then cultured in DMEM (FuHeng Biotechnology) containing 10% FBS (FuHeng Biotechnology) and 1% penicillin/streptomycin with 5% CO2 at 37℃.

Normal fibroblasts (NFs) and CAFs were isolated using fresh normal and CRC tissues as described previously [21]. NFs and CAFs were cultured in Exosome (Exo)-depleted DMEM/F12 medium (FuHeng Biotechnology) supplemented with 10% FBS for 48 h, then the culture medium was filtered using a 0.22 μM filter, and then suspended in isovolumetric 10% FBS-contained DMEM. Then the conditioned medium (CM) was collected, termly NF-CM and CAF-CM, and incubated for 2 days with LoVo and HCT-116 cells for further functional analyses.

Vector construction

The shRNA targeting METTL3 (sh-METTL3, 5'- AGGAGCCAGCCAAGAAATCAACTCGAGTTGATTTCTTGGCTGGCTCCT-3') and the scrambled shRNA (sh-NC, 5'- CCGGCAACAAGATGAAGAGCACCAACTCGAGTTGGTGCTCTTCATCTTGTTGTTTTTG-3'), and pcDNA3.1 overexpression METTL3 or acyl-CoA synthetase 3 (ACSL3) plasmids (METTL3 or ACSL3) and the empty plasmid (pcDNA) were designed by GenePharma (Shanghai, China). Finally, transient transfection was carried out in CAFs or CRC cell lines with the Lipofectamine 3000 (Invitrogen, Carlsbad, CA, USA).

Exosome isolation and co-culture

The CM of assigned NFs and CAFs were collected and centrifuged at 300 g for 10 min to obtain supernatant, which was then centrifuged at 10,000 g for 20 min and 100,000×g for 70 min. The precipitate was resuspended in 1×PBS, filtered with 0.22 μm strainer, and then subjected to centrifuge at 100,000×g for 1 h. Finally, exosomes were obtained and resuspended with PBS. Resuspended exosomes were lysed using the RIPA lysis buffer (Yeasen, Shanghai, China) on ice, then CD63 and TSG101 exosome markers were measured by western blotting. The morphology of exosomes was observed by a transmission electron microscope (TEM) (JEM-1010, JEOL, Tokyo, Japan), and the concentration and size distribution of exosomes were determined by nanoparticle-tracking analysis (NTA). For the co-culture model, 10 μg exosomes were resuspended in 100 μL 1 × PBS, and then incubated with CRC cell lines (1×105) for 24 h for further analyses.

MTT assay

LoVo and HCT-116 cells were reacted with 20 μL MTT (5 mg/ml) (Beyotime, Beijing, China) for 4 h in a 96-well plate (1×10^4 cells/well), and then incubated with DMSO to remove MTT crystals. Lastly, the absorbance was tested at 570 nm.

Colony formation assay

LoVo and HCT-116 cells were grown for 10–14 days in 6-well plates with 500 cells/well. After washing with PBS and staining, colonies (≥50 cells) were imaged and counted.

Transwell assay

LoVo and HCT-116 cells (1×105 cells/well) were placed into the upper chambers of the transwell inserts with 500 μL medium containing 10% FBS in the lower chamber. 24 h later, migrated cells were fixed and then dyed with crystal violet (Beyotime), followed by counting manually. For invasion analysis, the filters of the transwell chamber were pre-coated with DMEM-dissolved Matrigel and allowed to solidify for 1 h, and the other steps were the same as above.

Table 1 The primers for qRT-PCR

Name		Primers for qRT-PCR (5′-3′)
METTL3	Forward	CAGAGGCAGCATTGTCTCCA
	Reverse	ATGGACACAGCATCAGTGGG
SLC7A5	Forward	CATACGTTCGTCCCCTCGCA
	Reverse	GAATTCTGTATCGCTACGCCG
GAPDH	Forward	AGAAGGCTGGGGCTCATTTG
	Reverse	AGGGGCCATCCACAGTCTTC

Wound healing assay

LoVo and HCT-116 cells were cultured in 24-well plates with completed DMEM, and linear wound tracks were made when cells reached 80–90% confluency using a 1-ml pipette tip (0 h). After washing, cells were cultivated in a complete growth medium for 24 h. The wound distance was photographed at 0 and 24 h, and cell migration was assessed.

Western blotting

RIPA lysis buffer was utilized to isolate proteins, which were then loaded onto SDS-PAGE on 10% gels for separation and then transferred to nitrocellulose membranes. Thereafter, primary antibodies against GAPDH (ab181602, 1:5000) METTL3 (ab195352, 1:1000), PCNA (ab29, 1:5000), MMP9 (ab137867, 1:500), CD63 (ab271286, 1:1000), ASCL3 (ab166820, 1:1000) and TSG101 (ab125011, 1:2000) (Abcam, Cambridge, UK) were used to incubate for 12 h at 4℃. After incubation for 2 h at 37℃ with HRP-conjugated antibodies, protein bands were measured adopting the ECL kit (Beyotime).

Iron ion measurement

The intracellular levels of ferrous (Fe^{2+}) ions were measured as per the protocol of an iron assay kit (Abcam). In brief, LoVo and HCT-116 cells were lysed and incubated with the assay buffer for a half hour, followed by reacting with the iron probe for 1 h. Then the optical density was determined at 593 nm to assess Fe^{2+} levels.

Reactive oxygen species (ROS) detection

The supernatant of LoVo and HCT-116 cells was collected, and levels of intercellular ROS were measured by incubating with 2 μM DCFH-DA (Sigma-Aldrich, St. Louis, MO, USA) at 37℃for 30 min avoiding light. The fluorescent density was determined at 488 nM excitation and 525 nM emission.

Glutathione (GSH) detection

A Reduced glutathione (GSH) assay kit (Nanjingjiancheng, Nanjing, China) was adopted for the detection of GSH in LoVo and HCT-116 cells as per the manufacturer's protocol. The absorbance at 420 nm was examined by the spectrophotometer.

qRT-PCR

Total RNAs were isolated adopting Trizol (Takara, Dalian, China), then cDNAs were generated by reverse transcript using the PrimeScript™ RT kit (Takara), followed by qRT-PCR using cDNA template, primers (Table 1) and the SYBR Green Taq Mix (Takara) according to the recommended protocol. The relative level was assessed by the $2^{-\Delta\Delta Ct}$ method normalizing to GAPDH.

Total m6A detection

Total RNA was isolated using TRIzol from CRC cells, and then the EpiQuik m6A RNA Methylation Quantification Kit (EpiGentek, NY, USA) was adopted for the detection of total m6A contents in cells.

M^{6}A RNA immunoprecipitation (MeRIP) assay

LoVo and HCT-116 cells with indicated transfection or not were lysed using Trizol (Sangon Biotech) to obtain total RNAs, which were then fragmented by ultrasound. Thereafter, 1 μg smaller fragments were suspended in the immunoprecipitation buffer, and incubated with the 3 μg anti-IgG or anti-m6A antibody, RNase inhibitor, protease inhibitor and protein A magnetic beads at 4℃ for 2 h. Following proteinase K treatment, precipitated mRNAs were eluted and purified for qRT-PCR.

Dual-luciferase reporter assay

One m6A methylated site of ACSL3 was mutated (A-C mutant) by site-directed mutagenesis, then wild-type and mutated luciferase vectors were established using the pmir-GLO vectors (Promega, Beijing, China), named ACSL3 or ACSL3-MUT, which were then co-transfected into LoVo and HCT-116 cells with sh-METTL3 or sh-NC. Luciferase activities were detected after 48 h normalizing to the Renilla luciferase activities.

Animal experiments

This animal study was approved by the Ethics Committee of the Second Affiliated Hospital of Xi'an Jiaotong University. The sh-NC or sh-METTL3 was cloned into the pLentiLox 3.7 lentiviral plasmid (ATCC), and then transfected into 293T cells using the lipofectamine 3000. Afterwhile, cell supernatants were collected at 48 h and lentiviral particles were collected by ultracentrifugation (72,000 × g, 2 h). CAFs were incubated with lentiviral particles carrying sh-NC or sh-METTL3 in completed DMEM containing 8 μg/ml polybrene for 12 h, after washing with PBS, the CAF-exosomes were isolated, named sh-NC-CAF-exo or sh-METTL3-CAF-exo, and co-cultured with HCT-116 cells. Then 2×106 infected HCT-116 cells suspended in 40 μL PBS were subcutaneously injected into the back of the BALB/c nude mice (4–5 weeks old, n=5/each group, Slaike Jingda Laboratory, Hunan, China). The mice in the control group were injected with uninfected HCT-116 cells. In addition, when the nude mice generated tumors approximately 100 mm^3 in size, purified exosomes (sh-NC-CAF-exo or sh-METTL3-CAF-exo) or PBS were injected intratumorally twice weekly. Every 3 days, tumor volume was measured and then calculated by 0.5 × width^2 × length. At day 20, mice were killed, the tumors were isolated and weighed, then collected for western blotting analysis, or fixed in formalin for immunohistochemistry (IHC) analysis as described before [22]. For the lung metastasis model, 5×105 infected HCT-116 cells suspended in 100 μl PBS were injected intravenously in the tail vein into each 4-week-old mouse (n=5/each group). Three weeks later, the mice were sacrificed, and the lungs were isolated and fixed with phosphate-buffered formalin, and the number of metastatic nodules in the lungs was counted, followed by hematoxylin-eosin (HE) staining in the lung section.

Statistical analysis

The data were expressed as mean±standard deviation (SD). Statistical analyses were conducted using ANOVA (multiple groups) or Student's t test (two groups). $P<0.05$ suggested statistically significant.

Results

CAFs promote CRC cell proliferation, invasion and migration, and suppress cell ferroptosis

The conditioned medium (CM) of CAFs and NFs was collected, named NF-CM and CAF-CM, and then incubated with CRC cell lines to investigate the action of CAFs on CRC cell oncogenic phenotypes. Cells in the Control group were incubated with PBS. MTT and colony formation assays showed that CAF-CM incubation promoted LoVo and HCT-116 cell viability and colony formation ability, suggesting the enhancement of cell proliferation (Fig. 1A, B). In addition, CAF-CM incubation led to the boost of the migration and invasion of LoVo and HCT-116 cells (Fig. 1C-F). The related proteins were detected, western blotting analysis showed that levels of PCNA and MMP9 were increased in LoVo and HCT-116 cells with CAF-CM incubation (Fig. 1G, H), further suggesting the promotion of cell proliferation and mobility. Besides that, CRC cells were treated with 40 μM DMSO or Erastin (an inducer of ferroptosis) for 24 h, followed by NF-CM or CAF-CM incubation in Erastin-treated cells. As exhibited in Fig. 2A, Erastin suppressed the viability of LoVo and HCT-116 cells, which were rescued by CAF-CM incubation, but not NF-CM incubation. The biological characteristic of ferroptosis includes the accumulation of ROS and ions, as well as the exhaustion of GSH. Herein, the levels of Fe^{2+} and ROS were found to be increased, while GSH levels were decreased by Erastin treatment in CRC cells, while these effects mediated by Erastin were abolished after CAF-CM incubation (Fig. 2B-D), suggesting the inhibition of ferroptosis induced by CAFs.

m6A profiles and METTL3 expression were increased in CAFs and CRC cells

As shown in Fig. 3A, we found the m6A contents were up-regulated in LoVo and HCT-116 cells after CAF-CM incubation, implying that CAFs might function in CRC cells by mediating m6A modification. Thereafter, western blotting analysis showed that CAF-CM incubation

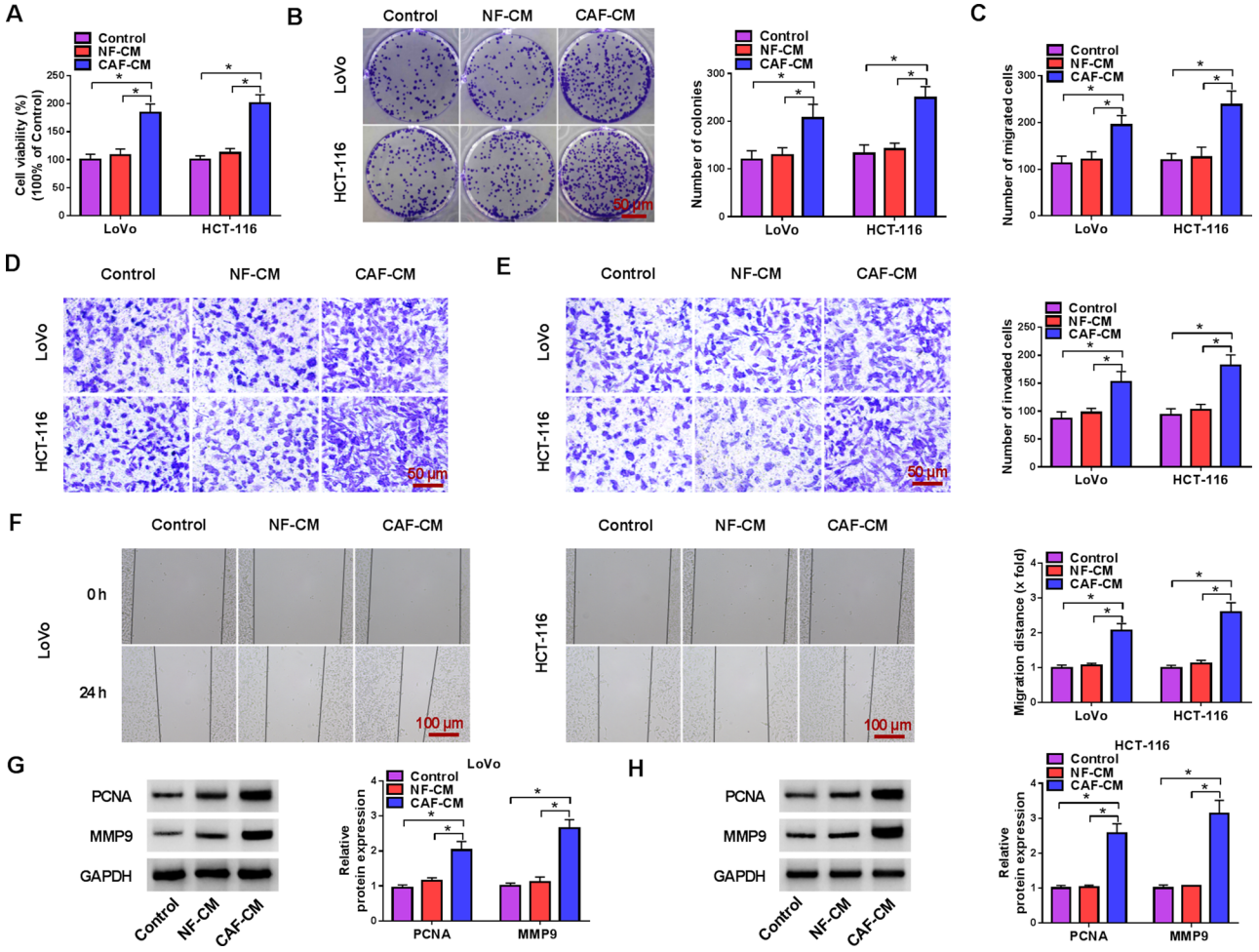

Fig. 1 CAFs promote CRC cell proliferation, invasion and migration,and suppress cell ferroptosis. (**A**-**H**) LoVo and HCT-116 cells were incubated with PBS, NF-CM or CAF-CM for 48 h. (**A**, **B**) MTT and colony formation assays for cell proliferation analysis. (**C**-**F**) Detection analysis of cell migration and invasion using transwell and wound healing assays. (**G**, **H**) Western blotting analysis for PCNA and MMP9 protein levels. Technical replicates ($n = 3$), biological replicates ($n = 3$), $^{*}P < 0.05$

but not NF-CM incubation markedly elevated METTL3 expression, but both CAF-CM and NF-CM incubation did not affect METTL14 expression in CRC cell lines (Fig. 3B, C). Moreover, METTL3 levels were higher in CAF-CM relative to NF-CM (Fig. 3D). Thus, we speculated that CAFs might function in CRC cells by mediating m6A modification through secreting METTL3. Then, TCGA and ENCORI databases showed that METTL3 levels were higher in colon cancer tissues compared with normal tissues (Fig. 3E, F). Furthermore, the high expression of METTL3 in clinical CRC tissues was observed (Fig. 3G, H). Also, METTL3 levels were up-regulated in CRC cell lines relative to the normal cells (Fig. 3I).

METTL3 is packaged into CAF exosomes

The exosomes were isolated from NFs and AFs, named NFs-Exo and CAFs-Exo. TEM data verified the morphology of exosomes (Fig. 4A). And exosomal markers (CD63 and TSG101) were detected by western blotting (Fig. 4B). In addition, NTA indicated a typical average exosome size distribution ranging from 100 to 180 nm (Fig. 4C). Then the expression profile of METTL3 in CAF exosomes was detected. As shown in Fig. 4D, the protein levels of METTL3 were higher in CAF exosomes than those in NF exosomes. Moreover, levels of METTL3 were increased in LoVo and HCT-116 cells after CAFs-Exo incubation compared with NFs-Exo (Fig. 4E). In addition, CAFs

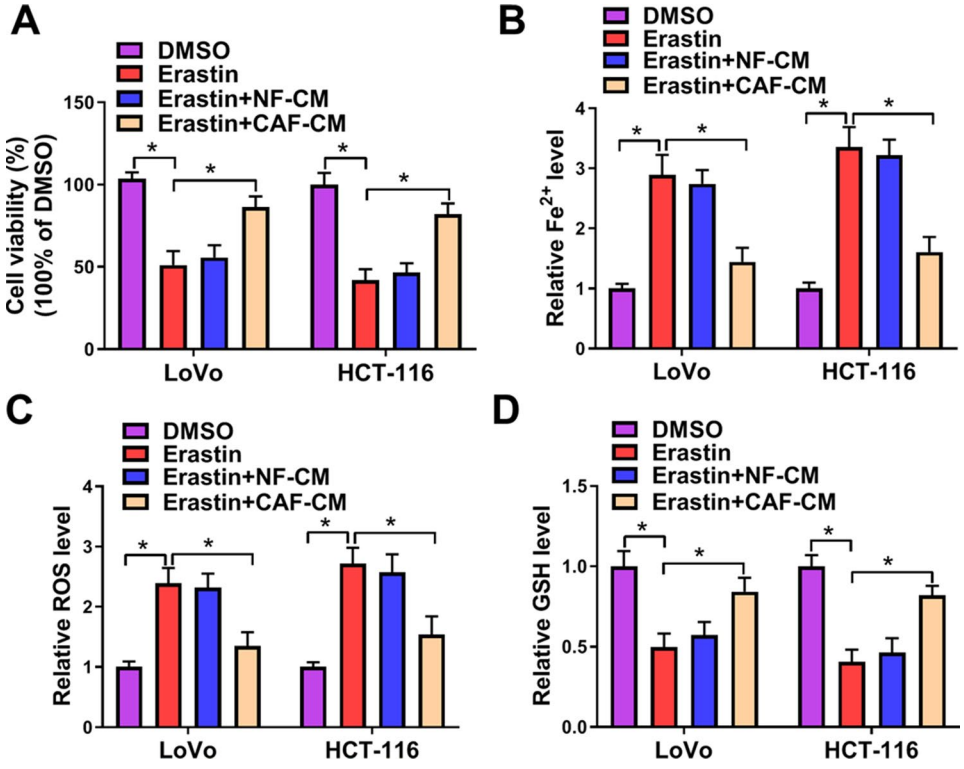

Fig. 2 CAFs suppresses CRC cell ferroptosis. (**A**-**D**) LoVo and HCT-116 cells were treated with 40 μM DMSO or Erastin for 24 h, followed by NF-CM or CAF-CM incubation in Erastin-treated cells for 48 h. **(A)** MTT assay for cell viability. (**B**-**D**) The accumulation of ROS and Fe^{2+}, and the exhaustion of GSH were detected using commercial kits. Technical replicates ($n = 3$), biological replicates ($n = 3$), $^*P < 0.05$

were treated with GW4869, an inhibitor of exosome biogenesis/release, or DMSO, then the culture medium was collected and incubated with LoVo and HCT-116 cells, it was found levels of METTL3 were decreased by GW4869 treatment (Fig. 4F), further indicating that METTL3 was secreted by exosomes of CAFs.

Knockdown of METTL3 in CAFs-exo suppresses CRC cell proliferation invasion and migration and induces cell ferroptosis

CAFs were transfected with sh-METTL3 or sh-NC, western blotting analysis showed that levels of METTL3 were decreased by sh-METTL3 in CAFs compared with sh-NC (Fig. 5A). Then exosomes were isolated from transfected CAFs, named sh-METTL3-CAFs-exo or sh-NC-CAFs-exo, and we found that levels of METTL3 were decreased in sh-METTL3-CAFs-exo relative to sh-NC-CAFs-exo (Fig. 5B). Thereafter, LoVo and HCT-116 cells were incubated with sh-METTL3-CAFs-exo or sh-NC-CAFs-exo for 24 h. Western blotting analysis showed that levels of METTL3 were decreased in CRC cells with sh-METTL3-CAFs-exo incubation (Fig. 5C). Functionally, sh-METTL3-CAFs-exo incubation suppressed the proliferation of LoVo and HCT-116 cells (Fig. 5D-F), as well as the migration and invasion of CRC cells (Fig. 5G-I and Fig. S1A, B). In addition, levels of PCNA and MMP9 were also decreased by sh-METTL3-CAFs-exo incubation in LoVo and HCT-116 cells (Fig. 5J, K). Besides that, sh-METTL3-CAFs-exo incubation caused the increases of Fe^{2+} and ROS production, but the decrease of GSH level in LoVo and HCT-116 cells (Fig. 5L-N), suggesting the boost of cell ferroptosis.

METTL3 induces ACSL3 m6A modification in CRC cells

According to the above data that METTL3 suppressed ferroptosis, we investigated whether METTL3 functioned in ferroptosis by regulating several key genes (GPX4, ACSL3, and SLC7A11) involved in the ferroptosis inhibition. The transfection efficiencies of sh-METTL3 or METTL3 were first validated using western blotting in CRC cell lines (Fig. 6A). Then we found that METTL3 knockdown markedly reduced ACSL3 levels in CRC cell lines (Fig. 6B, C). Moreover, we found that ACSL3 had rich m6A contents in LoVo and HCT-116 cells (Fig. 6D). TCGA and GEPIA databases exhibited a high expression of ACSL3 in colon cancer tissues (Fig. 6E, F). Also, a highly expressed ACSL3 in clinical CRC samples was observed (Fig. 6G), moreover, its expression was

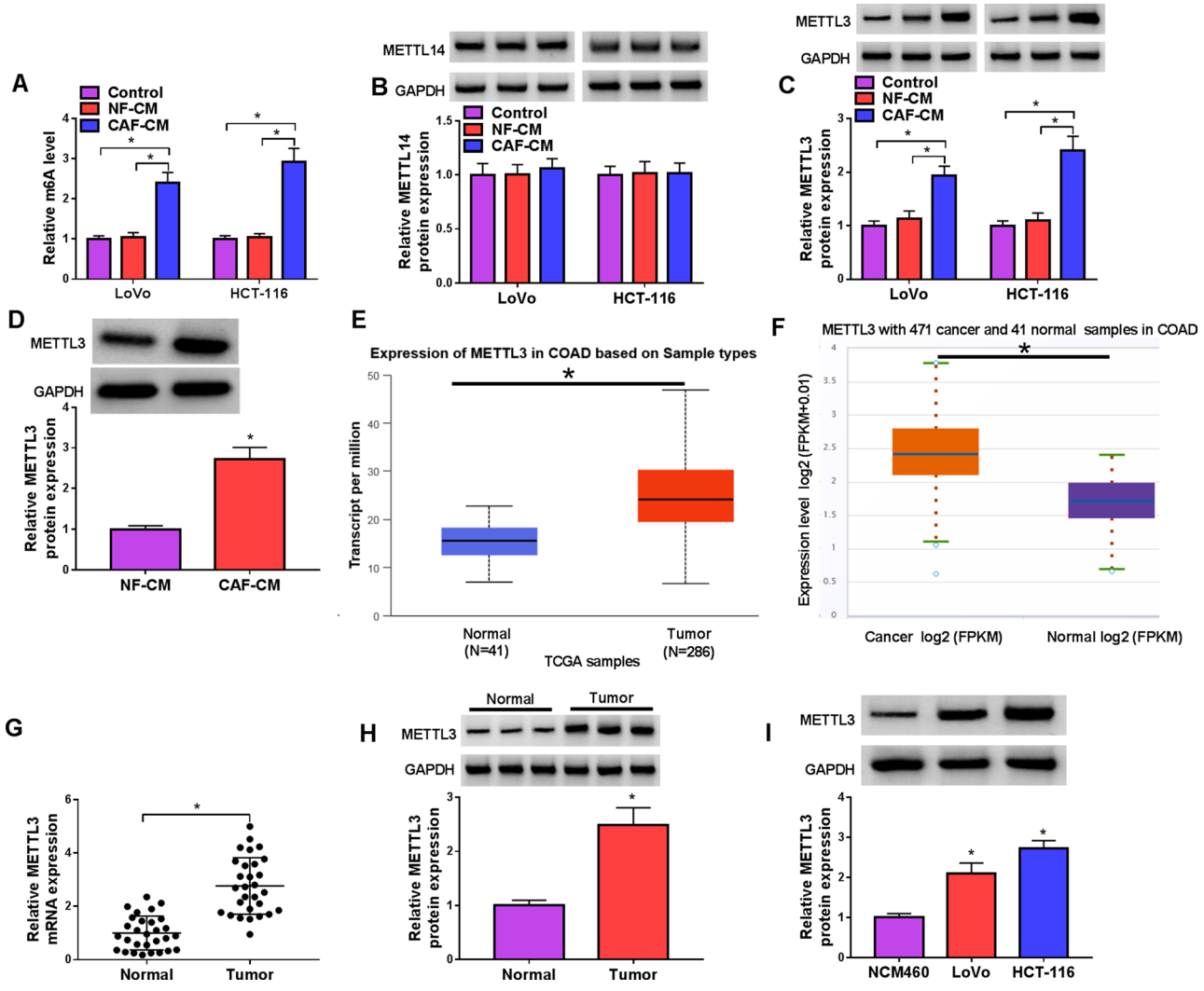

Fig. 3 m6A profiles and METTL3 expression were increased in CAFs and CRC cells. **(A)** The m6A contents were in LoVo and HCT-116 cells after CAF-CM incubation using the RNA m6A quantification kit. (**B**, **C**) Western blotting analysis for METTL3 and METTL14 levels in LoVo and HCT-116 cells after NF-CM or CAF-CM incubation. **(D)** Western blotting analysis for METTL3 expression in NF-CM or CAF-CM. (**E**, **F**) TCGA and ENCORI databases showed that METTL3 levels were higher in colon cancer tissues compared with the normal tissues (**G**, **H**) qRT-PCR and western blotting analyses for METTL3 levels in CRC tissues and matched normal tissues. **I** Western blotting for METTL3 protein levels in CRC cell lines and NCM460 normal cells. Technical replicates ($n = 3$), biological replicates ($n = 3$), $^*P < 0.05$

positively correlated with METTL3 expression level in CRC tissues (Fig. 6H). Thus, we speculated that METTL3 might mediate ACSL3 m6A modification. According to the SRAMP (http://www.cuilab.cn/sramp/), ACSL3 possesses m6A sites (Fig. 6I). Then we mutated one m6A site to conduct a dual-luciferase report assay. The results showed that METTL3 knockdown notably reduced the luciferase activity of the wild-type ACSL3 vector but not the mutated one in LoVo cells (Fig. 6J), indicating the interaction between METTL3 and ACSL3. Moreover, MeRIP and qRT-PCR assays showed that METTL3 knockdown could reduce the m6A content in ACSL3 in CRC cells (Fig. 6K). Besides that, METTL3 silencing reduced the stability of ACSL3 mRNA after Actinomycin D treatment, while METTL3 overexpression showed opposite effects (Fig. 6L, M). In addition, western blotting also showed that METTL3 silencing led to the decrease of ACSL3 expression, while METTL3 overexpression increased ACSL3 expression in LoVo and HCT-116 cells (Fig. 6N). Moreover, METTL3 silencing led to a decrease of ACSL3 expression in CAFs (Fig. S2A), and METTL3 deletion also reduced the stability of ACSL3 mRNA upon the Actinomycin D treatment in CAFs (Fig. S2B). In all,

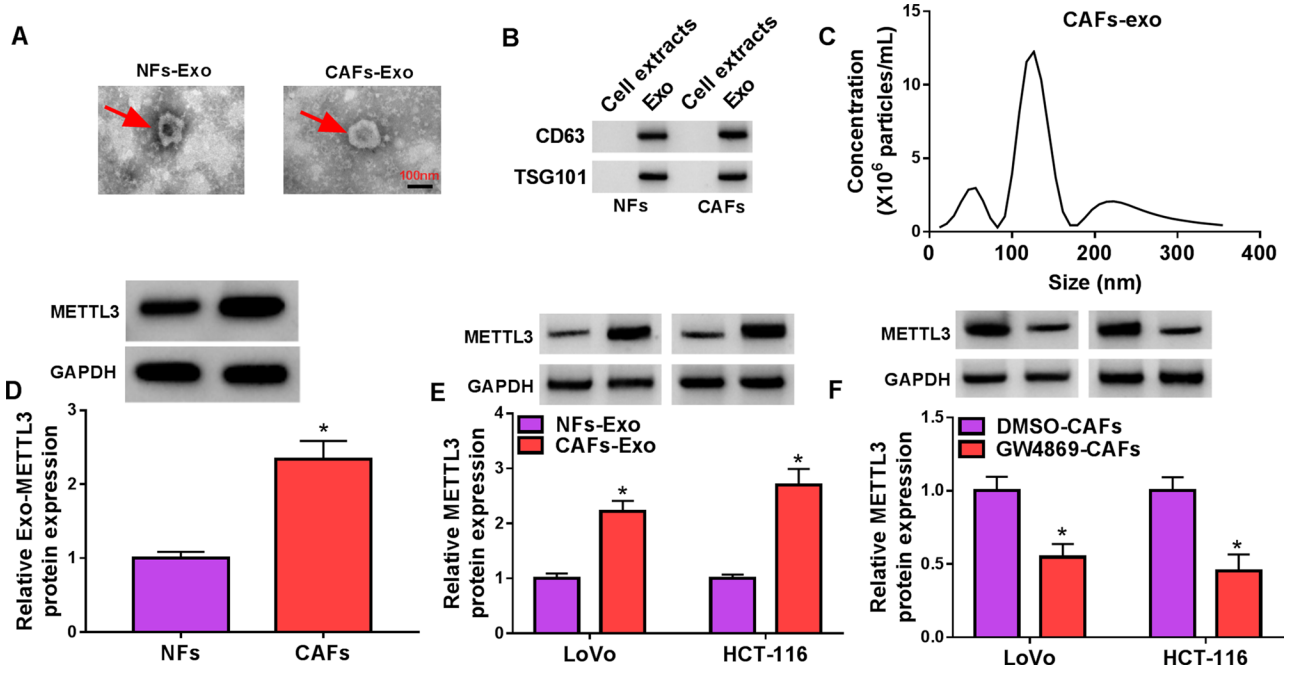

Fig. 4 METTL3 is packaged into CAF exosomes. **(A)** TEM verified the morphology of exosomes. **(B)** Western blotting analysis for exosomal markers (CD63 and TSG101) detection. **(C)** NTA indicated the exosome size distribution. **(D)** Detection of METTL3 expression in exosomes of CAFs or NFs by western blotting. **(E)** Levels of METTL3 were examined in LoVo and HCT-116 cells after 24 h of CAFs-Exo or NFs-Eco incubation. **(F)** Levels of METTL3 were examined in LoVo and HCT-116 cells after 48 h of incubation with the CM of GW4869- or DMSO-treated CAFs. Technical replicates ($n = 3$), biological replicates ($n = 3$),*$P < 0.05$

these data confirmed that METTL3 induced ACSL3 m6A modification to stabilize its expression.

Knockdown of METTL3 in CAFs-exo suppresses CRC cell proliferation invasion and migration and induces cell ferroptosis by ACSL3

Western blotting analysis showed that ACSL3 vectors markedly elevated ACSL3 expression in LoVo and HCT-116 cells (Fig. 7A), suggesting the elevation efficiency of ACSL3 vectors. Then LoVo and HCT-116 cells transfected with ACSL3 or pcDNA, followed by incubating with sh-METTL3-CAFs-exo or sh-NC-CAFs-exo for 24 h. Functionally, ACSL3 overexpression reversed sh-METTL3-CAFs-exo-induced inhibition of the proliferation (Fig. 7B, C), migration and invasion (Fig. 7D-F and Fig. S3A, B) of LoVo and HCT-116 cells. The down-regulation of PCNA and MMP9 protein levels in LoVo and HCT-116 cells was also rescued by ACSL3 overexpression (Fig. 7G, H). In addition, ACSL3 overexpression abolished sh-METTL3-CAFs-exo-evoked promotion of ferroptosis, evidenced by decreased Fe^{2+} and ROS levels, and increased GSH levels in LoVo and HCT-116 cells (Fig. 7I-K).

Knockdown of METTL3 in CAFs-exo impedes CRC growth and metastasis by regulating ACSL3

As exhibited in Fig. 8A, B, sh-METTL3-CAFs-exo treatment suppressed CRC tumor growth in vivo (reduced volume and light weight). Western blotting analysis showed that protein levels of METTL3, ACSL3, PCNA and MMP9 were decreased in tissues of the sh-METTL3-CAFs-exo group (Fig. 8C, D). IHC analysis also showed that the positive cells of PCNA, MMP9, METTL3 and ACSL3 were reduced in the sh-METTL3-CAFs-exo group (Fig. 8E). In addition, the number of metastatic nodules in the lung was higher in the sh-NC-CAFs-exo group, but reduced in the sh-METTL3-CAFs-exo group (Fig. 8F). Moreover, the results of HE staining showed that sh-METTL3-CAFs-exo led to the suppression of lung metastasis in mice (Fig. 8G).

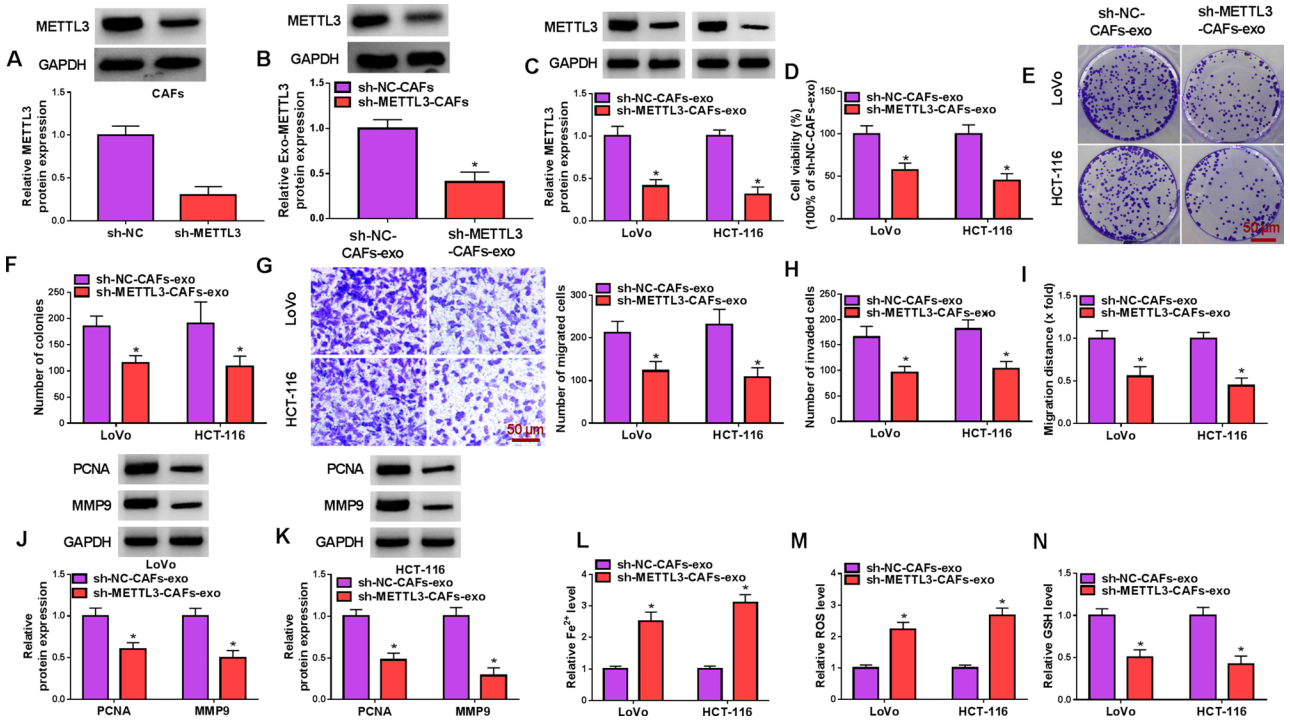

Fig. 5 Knockdown of METTL3 in CAFs-exo suppresses CRC cell proliferation invasion and migration and induces cell ferroptosis. **(A)** CAFs were transfected with sh-METTL3 or sh-NC, and levels of METTL3 in CAFs were examined by western blotting. **(B)** Exosomal METTL3 levels in CAFs transfected with sh-METTL3 or sh-NC were measured using western blotting. (C-N) LoVo and HCT-116 cells were incubated with sh-METTL3-CAFs-exo or sh-NC-CAFs-exo for 24 h. **(C)** Western blotting analysis for METTL3 expression in CRC cells. (**D**-**F**) MTT and colony formation assays for cell proliferation analysis. (G-I) Detection analysis of cell migration and invasion using transwell and wound healing assays. (**J**, **K**) Western blotting analysis for PCNA and MMP9 protein levels. (**L**-**N**) The accumulation of ROS and Fe^{2+}, and the exhaustion of GSH were detected using commercial kits. Technical replicates ($n = 3$), biological replicates ($n = 3$), $^*P < 0.05$

Discussion

In this work, we found that CAFs isolated from CRC samples could accelerate CRC cell proliferative, invasive and migratory abilities. Ferroptosis is an iron-dependent cell death highlighted by iron and ROS accumulation [23]. Through the use of ferroptosis inducer of Erastin, it was found CRC cell viability was reduced, and the accumulation of Fe2+and ROS was increased, while GSH levels were decreased in CRC cells, however, these effects were reversed by CAFs, suggesting that CAFs hindered cell ferroptosis. After incubation with the CM of CAFs, the m6A contents and METTL3 expression were increased in CRC cells. To investigate the manner in which CAFs affect CRC, exosomes were isolated from primary CAFs, we discovered that CAFs secreted METTL3 into CRC cells by packaging it into exosomes. Functionally, the deficiency of METTL3 in CAFs-exo restrained CRC cell proliferation, invasion and migration, and evoked cell ferroptosis in vitro, and impeded CRC growth and lung metastasis in nude mice. PCNA is a nuclear protein that regulates cell cycle and participates in DNA synthesis, which is commonly found significantly higher in various malignancies and commonly used as a marker of cell proliferation in cancers [24]. MMP9 is a significant protease that cleaves many ECM proteins to mediate basement membrane degradation, thereby supporting cancer invasion and metastases [25]. Here, we also found that the deficiency of METTL3 in CAFs-exo suppressed CRC cell proliferation, invasion and migration by decreasing PCNA and MMP9 expression in CRC cells.

Exosomes are nano-sized vesicles ranging from 40 to 150 nm in diameter, and are continually secreted from different cell types through exocytosis [26]. Exosomes are natural information carriers containing various biomolecules, such as lipids, nucleic acids, proteins, and other biomolecules, once secreted, exosomes may be taken up

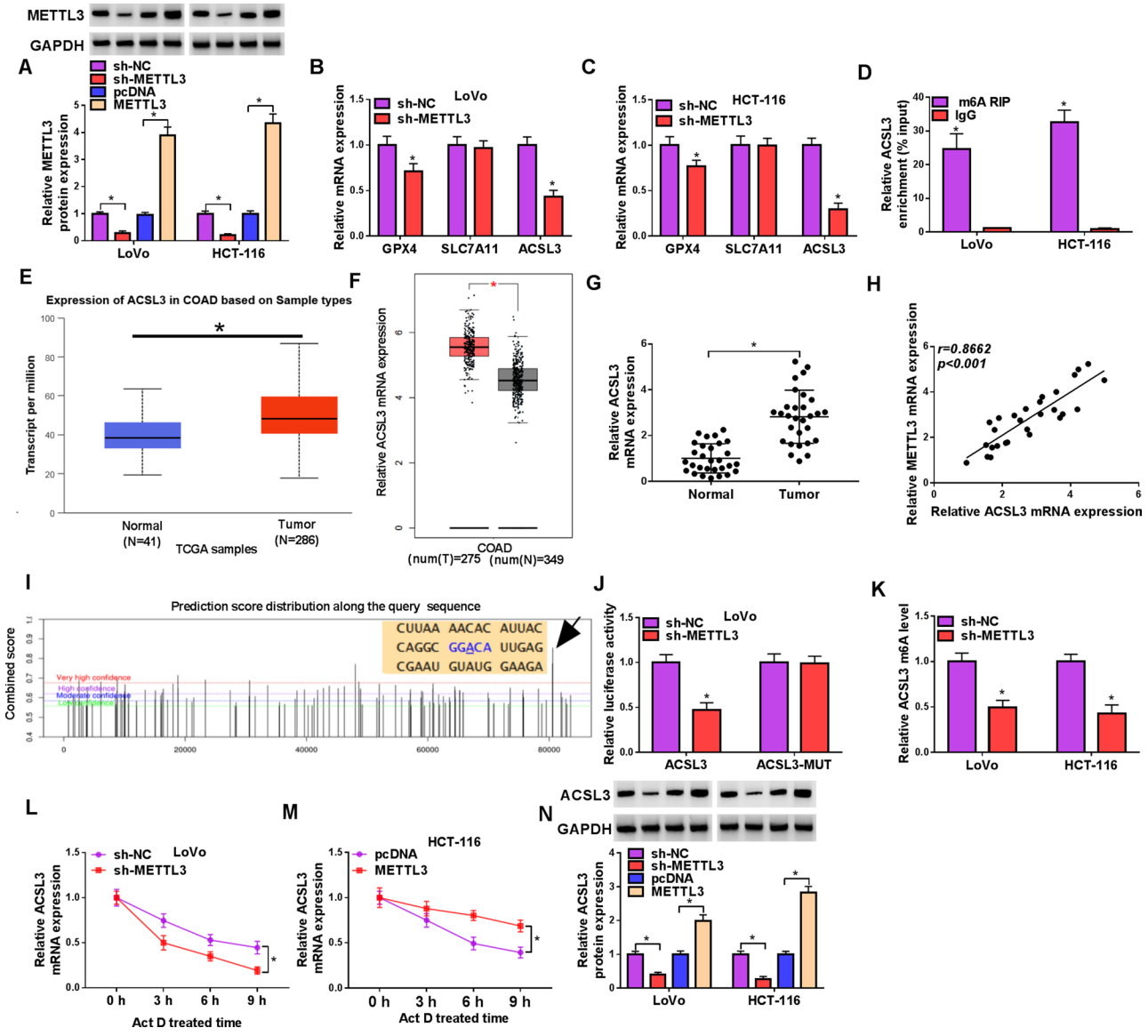

Fig. 6 METTL3 induces ACSL3 m6A modification in CRC cells. **(A)** The transfection efficiencies of sh-METTL3 or METTL3 were first validated using western blotting in CRC cell lines. (**B**, **C**) The effects of METTL3 knockdown on the expression of GPX4, ACSL3, and SLC7A11 in LoVo and HCT-116 cells. **(D)** MeRIP and qRT-PCR assays detecting ACSL3 expression in LoVo and HCT-116 cells. (**E**, **F**) TCGA and GEPIA databases exhibited a high expression of ACSL3 in colon cancer tissues. **(G)** Western blotting analysis for ACSL3 levels in CRC tissues and matched normal tissues. **(H)** Correlation analysis between ACSL3 and METTL3 expression in CRC tissues. **(I)** SRAMP (http://www.cuilab.cn/sramp/) predicts that ACSL3 possesses m6A sites. **(J)** Dual-luciferase report assay for the luciferase activity of wild-type or the mutant ACSL3 vector in LoVo cells after sh-METTL3 or sh-NC transfection. (K) MeRIP and qRT-PCR assays detecting the m6A content in ACSL3 after METTL3 knockdown in CRC cell lines. (**L**, **M**) The decay curve of ACSL3 mRNA was measured by Actinomycin D treatment in CRC cells after METTL3 down-regulation or overexpression. **(N)** Western blotting for ACSL3 expression in CRC cells after METTL3 down-regulation or overexpression. Technical replicates ($n=3$), biological replicates ($n=3$), $^*P<0.05$

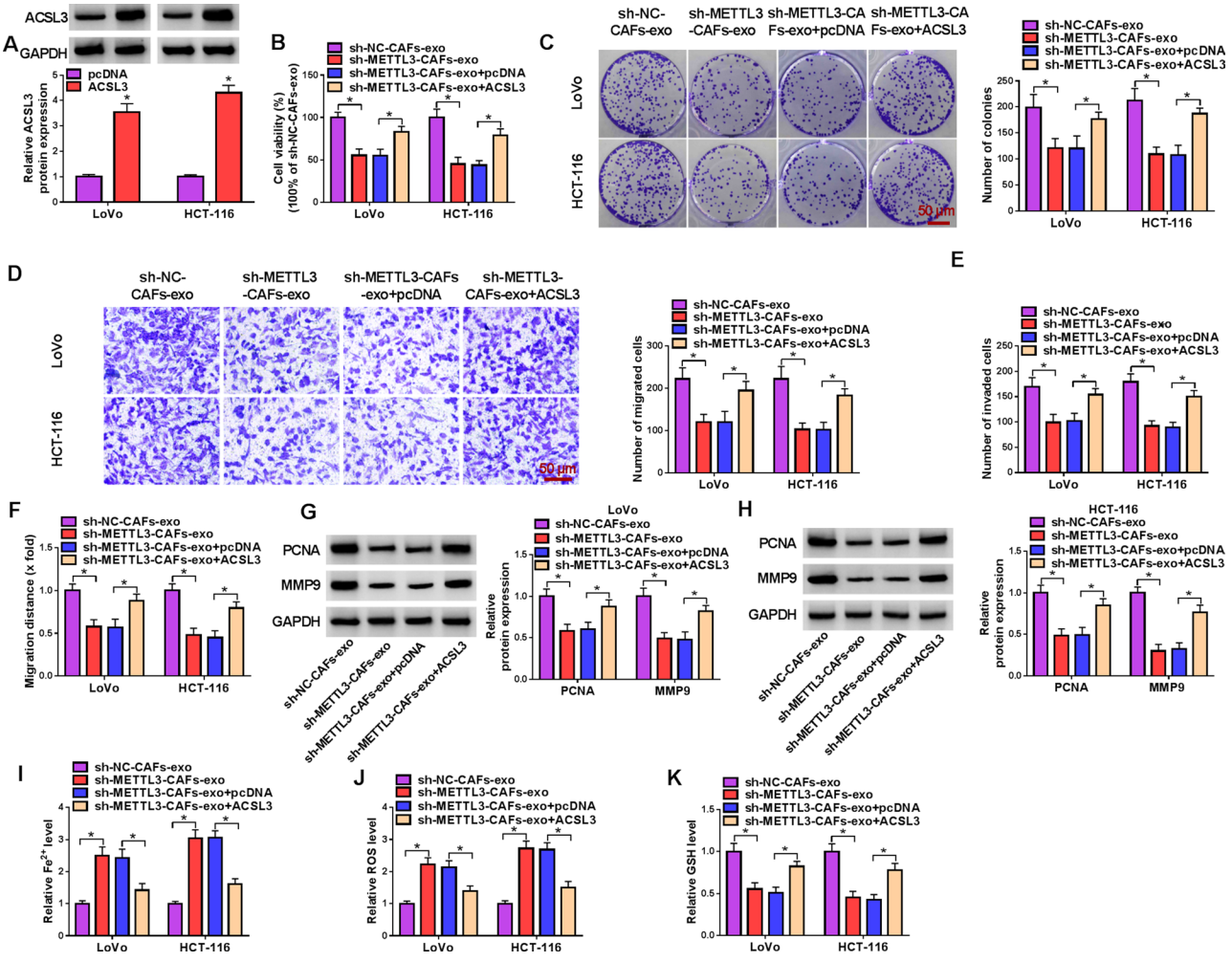

Fig. 7 Knockdown of METTL3 in CAFs-exo suppresses CRC cell proliferation invasion and migration and induces cell ferroptosis by ACSL3. **(A)** Western blotting analysis confirmed the elevation efficiency of ACSL3 or pcDNA vector. (**B**-**K**) LoVo and HCT-116 cells transfected with ACSL3 or pcDNA for 48 h, followed by incubating with sh-METTL3-CAFs-exo or sh-NC-CAFs-exo for 24 h. (**B**, **C**) MTT and colony formation assays for cell proliferation analysis. (**D**-**F**) Detection analysis of cell migration and invasion using transwell and wound healing assays. (**G**, **H**) Western blotting analysis for PCNA and MMP9 protein levels. (**I**-**K**) The accumulation of ROS and Fe^{2+}, and the exhaustion of GSH were detected using commercial kits. Technical replicates ($n = 3$), biological replicates ($n = 3$), $^{*}P < 0.05$

by donor cells, cells in local environments or travel to distant cells, where they communicate information through exosomal surface proteins and via the transmission of biofunctional cargoes, thereby affecting the behaviors of recipient cells [27–29]. Intercellular communication by exosomes plays a significant role in the physiological and pathological cellular processes [30–33]. In addition, due to the low immunogenicity and well tolerated, the ability to cross the BBB, the low-risk for cancer formation as well as the universal and stable presence in body fluids, exosomes are promising drug delivery carriers for conferring therapeutic efficacy [28, 34, 35]. Besides that, exosomes released from immune cells possess the ability to elicit immune responses, which has made them of particular interest in functioning as cell-free nanoscale vaccines for cancer immunotherapy [27, 36, 37]. Moreover, cancer-cell-derived exosomes are thought to have cancer-preferred delivery because of their homotypic characteristics [27]. Therefore, CAFs-derived exosomes combined with METTL3 shRNA may be a promising therapeutic strategy for CRC patients.

ACSL3 is an enzyme catalyzing esterification of fatty acids with Coenzyme A, and has been identified to be tightly relevant to ferroptosis by activating monounsaturated fatty acids, which competitively inhibits polyunsaturated fatty acid-induced iron ferroptosis [38]. In the cancer, MAT2A induced the production of S-adenosylmethionine, which increased ACSL3, thereby suppressing ferroptosis in gastric cancer [39]. FTO decreased the expression of anti-ferroptotic factors ACSL3 and GPX4 by inducing demethylation, thereby promoting ferroptosis in oral squamous cell carcinoma [40]. Moreover,

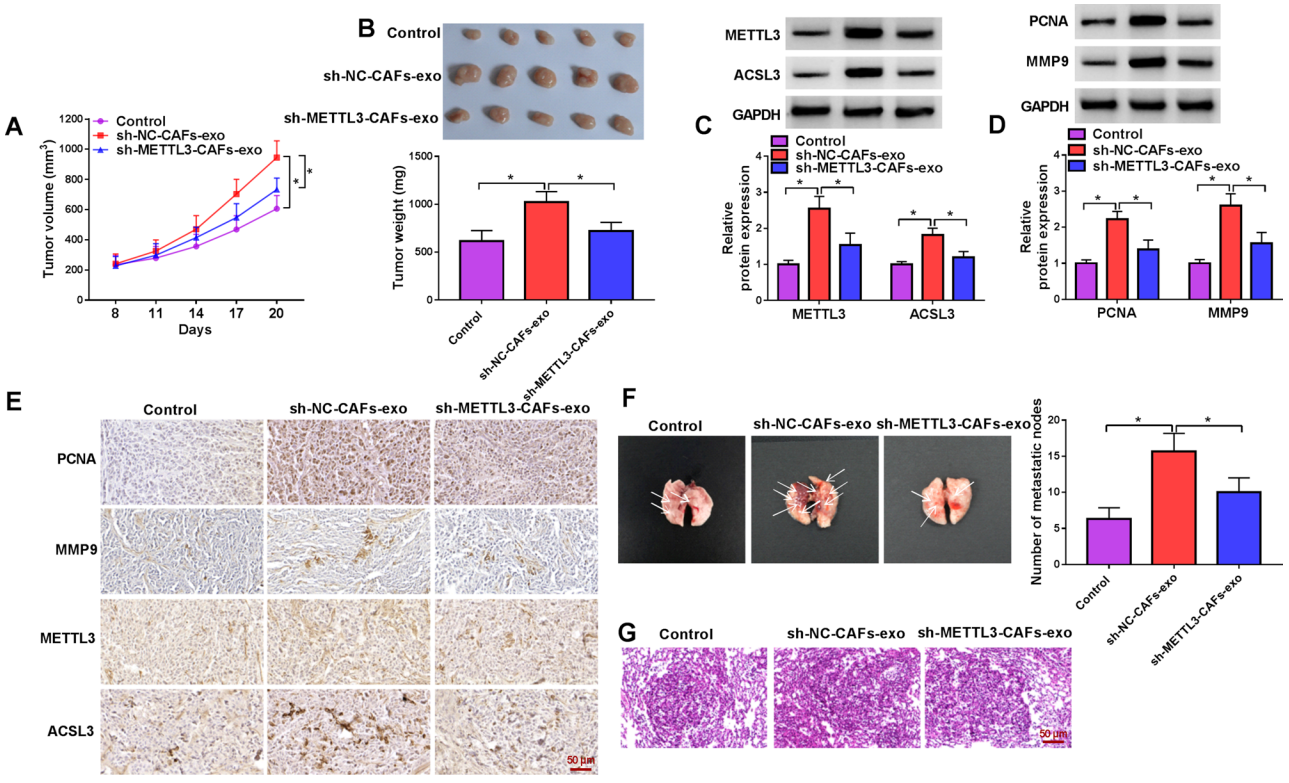

Fig. 8 Knockdown of METTL3 in CAFs-exo impedes CRC growth and metastasis by regulating ACSL3. (**A**, **B**) The growth curve of tumors **(A)**, the representative tumors and the weight of xenograft tumors **(B)**. (**C**, **D**) Measurement of METTL3, ACSL3, PCNA, and MMP9 protein levels in xenograft tumors in each group. **(E)** IHC analysis for METTL3, ACSL3, PCNA, and MMP9 positive cells in tumors of each group. **(F)** The number of metastatic nodules in the lung of each group. **(G)** Representative H&E staining of lung sections. Technical replicates ($n=3$), biological replicates ($n=5$), $^*P<0.05$

TGF-β1 up-regulated ACSL3 expression, which activated the fatty acid β-oxidation pathway to decrease NADPH and induce ATP production, and then promoted CRC metastasis [41]. In our study, we found ACSL3 had m6A sites and then verified that METTL3 induced ACSL3 m6A modification and stabilized its expression. Further functional analysis showed that ACSL3 overexpression abolished the proliferation and metastasis resistance, and ferroptosis sensitivity in CRC cells that caused by METTL3-decreased CAFs-exo.

In conclusion, METTL3 in exosomes derived from CAFs promoted the proliferation and metastasis and inhibited ferroptosis in CRC by eliciting ACSL3 m6A modification, providing a new insight into the development of exosome-based therapy in CRC.

Supplementary Information

The online version contains supplementary material available at https://doi.org/10.1186/s13062-024-00511-z.

Supplementary Material 1

Acknowledgements
None.

Author contributions
Hongtao Ren designed and performed the research; Mincong Wang, Xiulong Ma, Lei An, Yuyan Guo, Hongbing Ma analyzed the data; Hongtao Ren wrote the manuscript. All authors read and approved the final manuscript.

Funding
The present study was supported by Shaanxi social development science and technology research project(2021SF-138).

Data availability
No datasets were generated or analysed during the current study.

Declarations

Ethics approval and consent to participate
Written informed consents were obtained from all participants and this study was permitted by the Ethics Committee of Second Affiliated Hospital of Xi'an Jiaotong University.

Consent for publication
Not applicable.

Competing interests
The authors declare no competing interests.

Received: 21 May 2024 / Accepted: 8 August 2024
Published online: 19 August 2024

References

1. Sung H, Ferlay J, Siegel RL, Laversanne M, Soerjomataram I, Jemal A, Bray F. Global Cancer statistics 2020: GLOBOCAN estimates of incidence and Mortality Worldwide for 36 cancers in 185 countries. Cancer J Clin. 2021;71(3):209–49.
2. Dekker E, Tanis PJ, Vleugels JLA, Kasi PM, Wallace MB. Colorectal cancer. Lancet (London England). 2019;394(10207):1467–80.
3. Heiss JA, Brenner H. Epigenome-wide discovery and evaluation of leukocyte DNA methylation markers for the detection of colorectal cancer in a screening setting. Clin Epigenetics. 2017;9:24.
4. Xiao Y, Yu D. Tumor microenvironment as a therapeutic target in cancer. Pharmacol Ther. 2021;221:107753.
5. Arina A, Idel C, Hyjek EM, Alegre ML, Wang Y, Bindokas VP, Weichselbaum RR, Schreiber H. Tumor-associated fibroblasts predominantly come from local and not circulating precursors. Proc Natl Acad Sci USA. 2016;113(27):7551–6.
6. Sahai E, Astsaturov I, Cukierman E, DeNardo DG, Egeblad M, Evans RM, Fearon D, Greten FR, Hingorani SR, Hunter T, et al. A framework for advancing our understanding of cancer-associated fibroblasts. Nat Rev Cancer. 2020;20(3):174–86.
7. Maia A, Wiemann S. Cancer-Associated fibroblasts: implications for Cancer Therapy. Cancers 2021, 13(14).
8. Mao X, Xu J, Wang W, Liang C, Hua J, Liu J, Zhang B, Meng Q, Yu X, Shi S. Crosstalk between cancer-associated fibroblasts and immune cells in the tumor microenvironment: new findings and future perspectives. Mol Cancer. 2021;20(1):131.
9. Yang X, Li Y, Zou L, Zhu Z. Role of exosomes in Crosstalk between Cancer-Associated fibroblasts and Cancer cells. Front Oncol. 2019;9:356.
10. Peng Z, Tong Z, Ren Z, Ye M, Hu K. Cancer-associated fibroblasts and its derived exosomes: a new perspective for reshaping the tumor microenvironment. Mol Med (Cambridge Mass). 2023;29(1):66.
11. Li C, Teixeira AF, Zhu HJ, Ten Dijke P. Cancer associated-fibroblast-derived exosomes in cancer progression. Mol Cancer. 2021;20(1):154.
12. Chu X, Yang Y, Tian X. Crosstalk between pancreatic Cancer cells and Cancer-Associated fibroblasts in the Tumor Microenvironment mediated by exosomal MicroRNAs. Int J Mol Sci 2022, 23(17).
13. Qi R, Bai Y, Li K, Liu N, Xu Y, Dal E, Wang Y, Lin R, Wang H, Liu Z, et al. Cancer-associated fibroblasts suppress ferroptosis and induce gemcitabine resistance in pancreatic cancer cells by secreting exosome-derived ACSL4-targeting miRNAs. Drug Resist Updates: Reviews Commentaries Antimicrob Anticancer Chemother. 2023;68:100960.
14. Chen B, Sang Y, Song X, Zhang D, Wang L, Zhao W, Liang Y, Zhang N, Yang Q. Exosomal miR-500a-5p derived from cancer-associated fibroblasts promotes breast cancer cell proliferation and metastasis through targeting USP28. Theranostics. 2021;11(8):3932–47.
15. Shi W, Liu Y, Qiu X, Yang L, Lin G. Cancer-associated fibroblasts-derived exosome-mediated transfer of mir-345-5p promotes the progression of colorectal cancer by targeting CDKN1A. Carcinogenesis. 2023;44(4):317–27.
16. Xu W, Li J, He C, Wen J, Ma H, Rong B, Diao J, Wang L, Wang J, Wu F, et al. METTL3 regulates heterochromatin in mouse embryonic stem cells. Nature. 2021;591(7849):317–21.
17. Yue Y, Liu J, Cui X, Cao J, Luo G, Zhang Z, Cheng T, Gao M, Shu X, Ma H, et al. VIRMA mediates preferential m(6)a mRNA methylation in 3'UTR and near stop codon and associates with alternative polyadenylation. Cell Discovery. 2018;4:10.
18. Sun Y, Shen W, Hu S, Lyu Q, Wang Q, Wei T, Zhu W, Zhang J. METTL3 promotes chemoresistance in small cell lung cancer by inducing mitophagy. J Experimental Clin cancer Research: CR. 2023;42(1):65.
19. Xu Y, Bao Y, Qiu G, Ye H, He M, Wei X. METTL3 promotes proliferation and migration of colorectal cancer cells by increasing SNHG1 stability. Mol Med Rep 2023, 28(5).
20. Pan S, Deng Y, Fu J, Zhang Y, Zhang Z, Qin X. N6–methyladenosine upregulates miR–181d–5p in exosomes derived from cancer–associated fibroblasts to inhibit 5–FU sensitivity by targeting NCALD in colorectal cancer. Int J Oncol 2022, 60(2).
21. Yasuda T, Koiwa M, Yonemura A, Akiyama T, Baba H, Ishimoto T. Protocol to establish cancer-associated fibroblasts from surgically resected tissues and generate senescent fibroblasts. STAR Protocols. 2021;2(2):100553.
22. Yang Z, Zou S, Zhang Y, Zhang J, Zhang P, Xiao L, Xie Y, Meng M, Feng J, Kang L, et al. ACTL6A protects gastric cancer cells against ferroptosis through induction of glutathione synthesis. Nat Commun. 2023;14(1):4193.
23. Dixon SJ, Lemberg KM, Lamprecht MR, Skouta R, Zaitsev EM, Gleason CE, Patel DN, Bauer AJ, Cantley AM, Yang WS, et al. Ferroptosis: an iron-dependent form of nonapoptotic cell death. Cell. 2012;149(5):1060–72.
24. Ye X, Ling B, Xu H, Li G, Zhao X, Xu J, Liu J, Liu L. Clinical significance of high expression of proliferating cell nuclear antigen in non-small cell lung cancer. Medicine. 2020;99(16):e19755.
25. Huang H. Matrix Metalloproteinase-9 (MMP-9) as a Cancer Biomarker and MMP-9 biosensors: recent advances. Sensors 2018, 18(10).
26. Zhou R, Chen KK, Zhang J, Xiao B, Huang Z, Ju C, Sun J, Zhang F, Lv XB, Huang G. The decade of exosomal long RNA species: an emerging cancer antagonist. Mol Cancer. 2018;17(1):75.
27. Shao J, Zaro J, Shen Y. Advances in exosome-based drug delivery and Tumor Targeting: from tissue distribution to intracellular fate. Int J Nanomed. 2020;15:9355–71.
28. He C, Zheng S, Luo Y, Wang B. Exosome Theranostics: Biology and Translational Medicine. Theranostics. 2018;8(1):237–55.
29. Ludwig AK, Giebel B. Exosomes: small vesicles participating in intercellular communication. Int J Biochem Cell Biol. 2012;44(1):11–5.
30. Lugea A, Waldron RT. Exosome-mediated intercellular communication between stellate cells and Cancer cells in pancreatic ductal adenocarcinoma. Pancreas. 2017;46(1):1–4.
31. Roma-Rodrigues C, Fernandes AR, Baptista PV. Exosome in tumour microenvironment: overview of the crosstalk between normal and cancer cells. Biomed Res Int 2014, 2014:179486.
32. Milane L, Singh A, Mattheolabakis G, Suresh M, Amiji MM. Exosome mediated communication within the tumor microenvironment. J Controlled Release: Official J Controlled Release Soc. 2015;219:278–94.
33. Kosaka N, Yoshioka Y, Fujita Y, Ochiya T. Versatile roles of extracellular vesicles in cancer. J Clin Investig. 2016;126(4):1163–72.
34. Yang Y, Ye Y, Su X, He J, Bai W, He X. MSCs-Derived exosomes and Neuroinflammation, Neurogenesis and Therapy of Traumatic Brain Injury. Front Cell Neurosci. 2017;11:55.
35. Kalani A, Tyagi A, Tyagi N. Exosomes: mediators of neurodegeneration, neuroprotection and therapeutics. Mol Neurobiol. 2014;49(1):590–600.
36. Wang G, Hu W, Chen H, Shou X, Ye T, Xu Y. Cocktail Strategy based on NK Cell-Derived exosomes and their biomimetic nanoparticles for dual Tumor Therapy. Cancers 2019, 11(10).
37. Kalluri R, LeBleu VS. The biology, function, and biomedical applications of exosomes. *Science (New York, NY)* 2020, 367(6478).
38. Yang Y, Zhu T, Wang X, Xiong F, Hu Z, Qiao X, Yuan X, Wang D. ACSL3 and ACSL4, distinct roles in Ferroptosis and cancers. Cancers 2022, 14(23).
39. Ma M, Kong P, Huang Y, Wang J, Liu X, Hu Y, Chen X, Du C, Yang H. Activation of MAT2A-ACSL3 pathway protects cells from ferroptosis in gastric cancer. Free Radic Biol Med. 2022;181:288–99.
40. Wang Z, Li H, Cai H, Liang J, Jiang Y, Song F, Hou C, Hou J. FTO sensitizes oral squamous cell carcinoma to ferroptosis via suppressing ACSL3 and GPX4. Int J Mol Sci 2023, 24(22).
41. Quan J, Cheng C, Tan Y, Jiang N, Liao C, Liao W, Cao Y, Luo X. Acyl-CoA synthetase long-chain 3-mediated fatty acid oxidation is required for TGFβ1-induced epithelial-mesenchymal transition and metastasis of colorectal carcinoma. Int J Biol Sci. 2022;18(6):2484–96.

Publisher's Note